

## LAMOST Medium-Resolution Spectroscopic Survey

### (LAMOST-MRS): Scientific goals and survey plan

Chao Liu<sup>1,2</sup>, Jianning Fu<sup>3</sup>, Jianrong Shi<sup>4,2</sup>, Hong Wu<sup>4</sup>, Zhanwen Han<sup>5</sup>, Li Chen<sup>6,2</sup>, Subo Dong<sup>7,8</sup>, Yongheng Zhao<sup>4,2</sup>, Jian-Jun Chen<sup>4</sup>, Haotong Zhang<sup>4</sup>, Zhong-Rui Bai<sup>4</sup>, Xuefei Chen<sup>5</sup>, Wenyuan Cui<sup>9</sup>, Bing Du<sup>4</sup>, Chih-Hao Hsia<sup>10</sup>, Deng-Kai Jiang<sup>5</sup>, Jinliang Hou<sup>6,2</sup>, Wen Hou<sup>4</sup>, Haining Li<sup>4</sup>, Jiao Li<sup>5,1</sup>, Lifang Li<sup>5</sup>, Jiaming Liu<sup>4</sup>, Jifeng Liu<sup>4,2</sup>, A-Li Luo<sup>4,2</sup>, Juan-Juan Ren<sup>1</sup>, Hai-Jun Tian<sup>11</sup>, Hao Tian<sup>1</sup>, Jia-Xin Wang<sup>3</sup>, Chao-Jian Wu<sup>4</sup>, Ji-Wei Xie<sup>12,13</sup>, Hong-Liang Yan<sup>4,2</sup>, Fan Yang<sup>4</sup>, Jincheng Yu<sup>6</sup>, Bo Zhang<sup>3,4</sup>, Huawei Zhang<sup>7,8</sup>, Li-Yun Zhang<sup>14</sup>, Wei Zhang<sup>4</sup>, Gang Zhao<sup>4</sup>, Jing Zhong<sup>6</sup>, Weikai Zong<sup>3</sup> and Fang Zuo<sup>4,2</sup>

<sup>1</sup> Key Lab of Space Astronomy and Technology, National Astronomical Observatories, Chinese Academy of Sciences, Beijing 100101, China; *liuchao@nao.cas.cn*

<sup>2</sup> University of Chinese Academy of Sciences, 100049, China

<sup>3</sup> Department of Astronomy, Beijing Normal University, Beijing, 100875, China

<sup>4</sup> Key Lab of Optical Astronomy, National Astronomical Observatories, Chinese Academy of Sciences, Beijing 100101, China

<sup>5</sup> Yunnan Astronomical Observatory, China Academy of Sciences, Kunming, 650216, China

<sup>6</sup> Key Laboratory for Research in Galaxies and Cosmology, Shanghai Astronomical Observatory, Chinese Academy of Sciences, 80 Nandan Road, Shanghai 200030, China

<sup>7</sup> Department of Astronomy, School of Physics, Peking University, Beijing 100871, China

<sup>8</sup> Kavli Institute of Astronomy and Astrophysics, Peking University, Beijing 100871, China

<sup>9</sup> Department of Physics, Hebei Normal University, Shijiazhuang, 050024, China

<sup>10</sup> Space Science Institute, Macau University of Science and Technology, Taipa, Macau

<sup>11</sup> Center for Astronomy and Space Sciences, China Three Gorges University, Yichang, 443002, China

<sup>12</sup> School of Astronomy and Space Science, Nanjing University, Nanjing 210023, China

<sup>13</sup> Key Laboratory of Modern Astronomy and Astrophysics, Ministry of Education, Nanjing 210023, China

<sup>14</sup> College of Physics/Department of Physics and Astronomy, Guizhou University, Guiyang 550025, P.R. China

**Abstract** Since September 2018, LAMOST starts a new 5-year medium-resolution spectroscopic survey (MRS) using bright/gray nights. We present the scientific goals of LAMOST-MRS and propose a near optimistic strategy of the survey. A complete footprint is also pro-

survey is being conducted since 2018 and will be end in 2023. According to the detailed survey plan, we expect that LAMOST-MRS can observe about 2 million stellar spectra with  $R \sim 7500$  and limiting magnitude of around  $G = 15$  mag. Moreover, it will also provide about 200 thousand stars with averagely 60-epoch observations and limiting magnitude of  $G \sim 14$  mag. These high quality spectra will give around 20 elemental abundances, rotational velocities, emission line profiles as well as precise radial velocity with uncertainty less than  $1 \text{ km s}^{-1}$ . With these data, we expect that LAMOST can effectively leverage sciences on stellar physics, e.g. exotic binary stars, detailed observation of many types of variable stars etc., planet host stars, emission nebulae, open clusters, young pre-main-sequence stars etc.

**Key words:** stars: general—binaries: general—stars: variables: general—ISM: general—Galaxy: general—open clusters and associations: general

## 1 INTRODUCTION

LAMOST (Large Sky Area Multi-Object fiber Spectroscopic Telescope; also known as Guo Shou Jing telescope) is a 4-meter quasi-meridian reflective Schmidt telescope with 4000 fibers installed on its 5-degree-FoV focal plane. These configurations allow it to observe spectra for at most 4000 celestial objects simultaneously (Cui et al. 2012, Zhao et al. 2012). From 2011 to 2018, it has achieved its first stage low spectral resolution ( $R \sim 1800$ ) survey and obtained more than 10 million spectra, including about 9 million stellar spectra<sup>1</sup>. As one of the largest spectra database, LAMOST survey has shown substantial impact in diverse fields, from stellar astrophysics (Gao et al. 2014, Liu et al. 2015, Karoff et al. 2016, Luo et al. 2016, Wang et al. 2017, Ren et al. 2018, Liu 2019, Liu, J. et al. 2019, Gu et al. 2019), the Milky Way science (Tian et al. 2015, Xiang et al. 2015, Huang et al. 2016, Liu et al. 2017a, Liu et al. 2017b, Tian et al. 2017, Wang et al. 2017, Liang et al. 2018, Li et al. 2018, Tian et al. 2018, Wang et al. 2018, Xu et al. 2018, Yu & Liu 2018, Zhao et al. 2018, Li et al. 2019, Tian et al. 2019, Wang et al. 2019, Wang et al. 2019), to external galaxies and QSOs (Shen et al. 2016, Wu et al. 2010a, Wu et al. 2010b, Huang et al. 2019).

The 16 spectrographs installed on LAMOST has been upgraded during 2017 and currently support not only spectral resolutions of  $R \sim 1800$ , which is the same as the first stage survey, but also the new medium resolution with  $R \sim 7500$ . All spectrographs can be switched between the two modes during a day time to adopt different surveys.

At  $R \sim 7500$ , the blue and red cameras located on each spectrograph cannot cover wavelength ranges as large as the low resolution. Instead, the blue cameras can only cover the wavelength range from  $4950 \text{ \AA}$  to  $5350 \text{ \AA}$ , while the red cameras cover from  $6300 \text{ \AA}$  to  $6800 \text{ \AA}$ . With medium-resolution spectra, one can achieve the precision of the radial velocities to around  $1 \text{ km s}^{-1}$  for late type stars. The rotation of the stars can be well detected with uncertainty of around  $10 \text{ km s}^{-1}$  with the medium-resolution spectra. And the coverage of the wavelength enables to measure about 20 elemental abundances, including Li, C, Na, Mg, Si, Ca, Sc, Ti, V, Cr, Mn, Fe, Co, Ni, Cu, Ba, Y, Sm, and Nd. In the mean time, the red part of the spectra can well cover  $H\alpha$ , [NII], and [SII] emission lines, which is crucial for the science related to the Galactic

nebulae, such as the HII regions, the supernova remnants, the planetary nebular etc. The H $\alpha$  profile is also very important in research on the proto-planetary disk surrounding the very young stars.

Since October 2018, LAMOST started the second stage survey program, LAMOST II, which contains both low- and medium-resolution spectroscopic surveys. LAMOST II will take around 50% nights (dark/gray nights) to continue the previous low-resolution spectroscopic survey. The other 50% nights (bright/gray nights) are assigned for medium-resolution survey. While the scientific goals of the LAMOST II low-resolution survey is generally the same as the first 5-year survey (Deng et al. 2012), the new medium-resolution survey (hereafter MRS) will aim for new goals, including Galactic archaeology, stellar physics, star clusters, star formation, exoplanet host stars, Galactic nebulae etc.

Among these scientific goals, synergy with other international space-based surveys can manifest the impact of the MRS survey. In the past few years, *Kepler* (Borucki et al. 2010) and K2 missions have provided accurate time-domain photometric data for hundreds of thousands of stars distributed in lots of fields in the sky. These data are invaluable legacy in many topics from exoplanet to asteroseismology. As its successor, NASA Transiting Exoplanet Survey Satellite (TESS, Ricker et al. 2014) launched in April 2018 and will conduct a two-year survey of nearly the entire sky to search for planets around bright main-sequence stars, potentially yielding thousands of new exoplanet discoveries including those smaller than the Neptune. In the mean time, the time-domain data are also extremely critical for asteroseismology, pulsators, and binary stars. Ground-based spectroscopic data for a large number of *Kepler*, *K2*, and TESS observed stars will remarkably extend the science of these missions and are expected to substantially amplify the science impacts.

The *Gaia* satellite has been launched by ESA since December 2013 and the *Gaia* DR2 data have been publicly released since April 25 2018 (Gaia Collaboration et al. 2016, Gaia Collaboration et al. 2018). The final data release will be expected to come out in 2022. As an ambitious mission, *Gaia* has provided extremely accurate astrometry as well as photometry for 1.7 billion stars with *G* band magnitude brighter than 20.7 mag<sup>2</sup>. In the next decades, *Gaia* will be the one of the most important data legacy in almost all fields of astronomy.

The high-cadence high-precise time-domain photometric data, extremely precise trigonometric parallaxes and proper motions combined from these space missions will be perfect supplementary of the LAMOST-MRS survey, which can provide precise radial velocities, stellar rotations, atmospheric parameters, elemental abundances, and time-domain spectroscopic data.

In this paper, we propose the scientific goals of the LAMOST-MRS and the targeting and survey plans. Section 2 describes the proposed scientific goals. Section 3 provides a brief report of the test observing with mid-resolution spectrographs and a simulation of the survey to find the approximately optimistic solution of the survey such that all scientific goals can be satisfied. Section 4 gives the detailed sky footprint and targeting plan. And Section 5 gives a brief summary.

## 2 SCIENTIFIC GOALS

As a stellar medium-resolution spectroscopic survey for millions of stars, LAMOST-MRS aims at diverse scientific goals, including

- Binarity/Multiplicity,
- Stellar pulsation,
- Star formation,
- Emission nebulae,
- Galactic archaeology,
- Host stars of exoplanets,
- Open clusters.

In the next sub-sections, we briefly introduce these scientific goals one by one.

### 2.1 Binarity

More than 50 percent of stars are in binary or multiple systems in the Milky Way (Duchene & Kraus 2013). The binary interactions can dramatically affect the evolutionary tracks of both components in binary systems. Therefore the binary evolution, even in main-sequence stage, can be significantly different from single-star evolution (Jones & Boffin 2017).

A number of outstanding scientific questions are related to binary stars. Massive binaries containing O or B-type stars are linked to the black hole/neutron star binaries, which are considered as sources of gravitational wave (Abbott et al. 2016, De Marco & Izzard 2017). Binaries composed of a white dwarf and a A, F, G or K type main-sequence star or composed of two white dwarfs are likely the progenitors of cosmologically important type Ia supernovae (Webbink 1984, Han & Podsiadlowski 2004). Meanwhile, it has been widely known that binary evolution produces most exotic stellar objects e.g. hot subdwarf stars, barium stars, symbiotic stars, double degenerates, cataclysmic variables, AM CVn stars, binary millisecond pulsars, bipolar planetary nebulae, extremely low-mass white dwarfs, etc (Han et al. 1995, Han et al. 1995, Han 1998, Han et al. 2002, Han & Podsiadlowski 2004, Chen & Han 2009, Chen et al. 2013, Chen et al. 2017, Li et al. 2019). However, several crucial processes in binary evolution such as mass and angular momentum loss, dynamical mass transfer and common envelope evolution etc. have not been well understood yet. These processes determine the formation of the exotic objects and the ultimate fate of a binary. Searching for some of the exotic objects (they are actually binaries in various evolutionary stages) and determining their physical properties are greatly helpful in understanding the important processes in binary evolution, then the formation of type Ia supernovae and sources of gravitational waves.

In addition to the highly interesting exotic binaries, the statistical properties of the binaries in the field as well as in stellar systems (open clusters, globular clusters, associations etc.) are also of importance in the sense that they can provide critical information of the formation and evolution of the binary systems. The fraction of binaries in a stellar population can vary with metallicity (Raghavan et al. 2010, Gao et al. 2014,

Duchêne & Kraus 2013). In the mean time, the distribution of the mass-ratio of binaries are also different in binary systems with different primary mass (Duchêne & Kraus 2013, Liu 2019). The distribution of the period of binaries in the solar neighborhood is unveiled by various works (Duquennoy & Mayor 1991, Raghavan et al. 2010). It is not clear, however, whether this period distribution is universal. It is also found that the orbital eccentricity is averagely small at small period, implying that most of the orbits of close binaries have been circularized. According to various simulations (Kratter et al. 2008, Machida et al. 2009, Kratter et al. 2010, Tanaka & Omukai 2014, Moe & Kratter 2018), it seems that, the close binaries are formed from disk fragmentation, which can lead to the anti-correlation between the binary fraction and metallicity, while some observational evidence hints that the wide binaries may have different channel of formation (El-Badry & Rix 2019, Tian et al. 2019, El-Badry et al. 2019). Moreover, it has been showed that, at the early stage when the field stars were still staying in the embedded clusters in which they were born, the dynamical process has already effectively changed the statistical properties of the binaries by stripping out the smaller and distant companions of the binaries (Marks & Kroupa 2011, Liu 2019).

With LAMOST-MRS survey, we expect to discover more exotic binaries under different evolutionary stages, such as CVs, Hot subdwarf stars, WD+MS binaries, symbiotic stars, barium stars, the PNe with binary central stars, etc. Medium-resolution spectra with accurate measurement of the radial velocities enables to derive their physical and orbital parameters in high precision. These are crucial in understanding common-envelope phase, the formation of SN Ia, and gravitational wave sources. We can more precisely obtain the orbital parameters of eclipsing binaries combined by the time-domain photometric light curves and LAMOST radial velocity curves.

We can also determine the behavior (single or double emissions, absorption) of the  $H\alpha$  lines. Using LAMOST MRS time-domain data, we can study the time or orbital phase evolution of the  $H\alpha$  lines, especially short-time scale variation. It is possible for late-type eclipsing binaries to detect the plage or flare events from  $H\alpha$  line variation. We can compare the activity fraction of single or binary system and discuss the effect by the close companion (Morgan et al. 2012). Starspots and energy of flares derived from time-domain photometric data will be complementary to the spectroscopic features (Zhang et al. 2020). Finally, we can determine the relationship of photometric and chromospheric activity for late-type eclipsing binaries. This will promote the exact mechanism behind the magnetic field generation of late-type eclipsing binaries.

Meanwhile, the multi-epoch MRS survey for a large number of stars with different spectral types allows us to accurately count the binary fraction, mass-ratio distribution, and orbital eccentricity distribution for close binaries with period smaller than around one thousand days. In fact, for many of these stars, we are able to partly solve their orbital parameters from their radial velocity curves. Moreover, we expect that a fraction of these spectroscopic binaries are double-line binaries (SB2), which orbital parameters can be completely solved out from their radial velocity curves. As a by-product, we are able to provide the accurate stellar mass for a few thousands of stars with different spectral types.

Combined with time-domain photometric data, such as TESS, *Kepler*, and ZTF (Masci et al. 2019), more information can be provided especially for the eclipsing binaries. These will be a large amount of invaluable

## 2.2 Variable stars

Stellar pulsations provide the unique technique for one to probe the internal structures and chemical compositions of stars by means of asteroseismology (Aerts et al. 2010). The well-defined internal physics of stars may inversely offer precise information to constrain stellar evolutionary theory (e.g., Giammichele et al. 2018). Currently, most of the asteroseismic data are purely from high-precision high-cadence time-domain photometric data, such as *Kepler* and TESS. However, lack of the precise measurement of the stellar atmospheric parameters, including the effective temperature, surface gravity, metallicity, and rotation, will limit many studies in asteroseismology. Successful experience from past years suggests that LAMOST is an ideal instrument for follow-up observations of those spaceborne surveys (e.g., De Cat et al. 2015, Zong et al. 2018)

With the LAMOST-MRS, precise atmospheric parameters will be obtained for various types of stars, which will reduce the parameter space when searching for the optimal seismic models, in particular for large amplitude pulsators. The time-series variations of radial velocity from LAMOST-MRS, together with the light curves derived from the high-precision photometry, will offer better constraints on the determination of stellar parameters, including the dynamical processes of pulsating stars as well as the masses and radii of the components for binaries (Murphy et al. 2018).

LAMOST-MRS will help to provide an independent measurement of the rotation periods of stars which have been also estimated from the *Kepler* photometry. It is also helpful to determine the intensity of stellar activity on the surface using the particular emission lines.

These topics can get benefit from time-domain spectroscopic observations for a large amount of target stars, especially when high-precision long-time-coverage light curves, e.g. the observations from *Kepler* and *K2* campaigns, are available.

## 2.3 Star forming regions

The detailed process of star formation is far from clear. In general, the young stars are mostly born in clusters embedded in molecular clouds (Lada, & Lada 2003). After a fairly short time scale, most of the young embedded clusters are disrupted and stars are scattered into the field. It is of high interests that how young stars co-evolve with the molecular clouds and how they are decoupled (Stutz & Gould 2016). Another interesting question is the binary fraction in the young stellar populations. The comparison between the very young and old stellar populations is important to understand whether the binary stars have been experienced substantial dynamical processing during their stay in the embedded clusters (Marks & Kroupa 2011, Liu 2019). Young low-mass stars may still keep a weak proto-planetary disk surrounding the star. This can be observed from the emission of the H $\alpha$  line. The variation of the emission line profiles can provide detailed properties of these disks. Moreover, the evolution of the Lithium in the atmosphere of young stars is also an interesting open question, which is related to the cosmological evolution of Lithium.

LAMOST-MRS will cover a few nearby star forming regions, such as Taurus, Orion, Perseus, Gemini etc., and a dozen of star associations. We will sample these regions and obtain medium-resolution spectra

disks in optical band with LAMOST-MRS spectra. Moreover, because the LAMOST-MRS spectra contains Li line at  $6707\text{\AA}$ , it allows us to approximate the evolution of the Lithium in the young stars.

## 2.4 Galactic Archaeology

It is of great importance to unravel the formation and evolutionary history of the Milky Way key of which includes reconstructing the lost stellar substructures of the early Galaxy. Although impossible to identify them from the spatial distributions, as stellar abundances reflect the chemical state of the gas where stars have been born, remnants of the disrupted yet now-dispersed ancient building blocks, e.g. dwarf galaxies and globular clusters, shall be identified through exploring their stellar chemistry although it is impossible to identify them from the spatial distributions. Kinematic properties can be a critical supplementary to chemical tagging when one take into account the accurate astrometry from *Gaia* catalog. Chemical-kinematic tagging will finally provide an comprehensive view of the ensemble of the Milky Way in the context of the near field cosmology.

The LAMOST-MRS will observe around a million medium-resolution spectra for FGK stars. These enables us to measure around 20 elemental abundances, including light proton-capture elements,  $\alpha$ -elements, odd-Z elements, iron-peak elements, and neutron-capture elements, in reasonable precision (Zhang et al.2019, Zhang et al.2020). which would be sufficient to represent the main nucleosynthetic processes in both dwarf and giant stars, and allow chemical tagging of individual stars to their original formation event. Combining with the radial velocities with uncertainty of around  $1\text{ km s}^{-1}$  and *Gaia* astrometry, which will permit differentiation of stars by their kinematics, we will be able to reconstruct the original stellar building blocks, and to investigate the history of the formation and evolution of the Galaxy by means of chemical-kinematic tagging.

## 2.5 Emission nebulae

The emission nebulae include planetary nebulae (PNe), HII regions, supernovae remnants (SNRs), Herbig-Haro (HH) objects etc (Wu et al. 2020). These objects have various scientific interests covering the nature of the ionized gas, star formation and the evolution of the Milky Way.

The three-dimensional ionized structures of PNe reflect various nebular expansion velocities. The interesting scientific questions on PNe include 3D ionized structures and electron density distributions of Galactic PNe, the evolution of various morphological PNs, and the chemical abundance of our Galaxy traced by PNe.

HII regions are gas nebulae ionized by high-energy radiation (mostly are ultraviolet photons) from young massive stars. As the distribution of these stars and the surrounding gas are irregular, in most situation, the shape of the HII regions is far from simple Strömgren sphere, instead, they often appear clumpy and filamentary (Monreal-Ibero et al. 2011). HII regions are natural laboratories for studying star-forming actives and interactions between the massive stars and surrounding ISM (Mao et al. 2018). Meanwhile, the spatial variation of chemical abundances across the Galactic disk can also be well measured with HII regions (Simpson et al. 1995, Afflerbach et al. 1997, Deharveng et al. 2000, Esteban et al. 2005,

SNRs are the material ejected in an explosion of SN, which can continue their life through interaction with the surrounding interstellar medium (ISM) for thousands or even up to a million year. They are important sources of the injection of energy and heavy elements into the interstellar medium, and are believed to be the possible sources of the Galactic cosmic rays. Moreover, SNRs probe the immediate surroundings of supernovae, shaped by their progenitors. The main features of SNRs are strong shock waves, amplified magnetic field, ultra-relativistic particles (cosmic rays) generation and associated synchrotron radiation (Arbutina 2017).

HH objects (Ambartsumian 1954) are formed when narrow jets of partially ionized gas ejected by stars collide with nearby gas and dust at speeds of several hundred kilometers per second. They are small-scale shock regions intimately associated with star forming regions (Schwartz 1983) and can trace supersonic shock waves (Bally 2016), often found in large groups, and some can be seen around a single star, aligned with its rotational axis.

LAMOST-MRS will be used as a super large IFU when observe a large area of the emission nebulae, and to provide high quality medium-resolution spectra containing most of the prominent emission lines e.g.  $H\alpha$ , [NII], [SII], [OIII] etc. The emission nebulae can be well discriminated from the  $\log(H\alpha/[N II])$  vs.  $\log(H\alpha/[S II])$  (S2N2) diagnostic diagram (Hsia & Zhang 2014). LAMOST-MRS will obtain large number of optical spectra of H II regions in the Galactic disk, which allow us to study the radial abundance gradient and to re-check whether there is evidence of flaring at the outer disk (Wang et al. 2018). We will focus on a dozen of largely extended SNRs and efficiently map their details with the help of the wide field-of-view, multi-fibers, and high-precision in emission line profiles provided by LAMOST-MRS (Ren et al. 2018). LAMOST-MRS will provide opportunity to study the most of known HH objects in details and identify more HH objects candidates.

## 2.6 Host Stars of Exoplanet and Synergy with TESS

Both *Kepler* and TESS are imaging surveys aiming to exoplanets detection from transit method. For the transit method, the accurate knowledge of the host stars is crucial to characterize the exoplanets and study the dependence of their distribution on the stellar environment. The data of the LAMOST-MRS survey will offer a great synergy with TESS by providing a large and complete spectroscopic sample of exoplanet host stars as well as the parent control samples for population studies.

Previous studies (see, e.g., Dong et al. 2014, Xie et al. 2016, Wang et al. 2016) have demonstrated that the stellar parameters (Luo et al. 2015) derived from LAMOST low resolution spectroscopic observations of the *Kepler* field (De Cat et al. 2015, Ren et al. 2016) reach high precision for main sequence stars ( $\sigma_{[Fe/H]} \approx 0.1$  dex,  $\sigma_{\log(g)} \approx 0.1$  dex). The large and unbiased LAMOST-*Kepler* sample with well characterized stellar properties have led to many new insights into *Kepler* planets and their distributions, including (not limited to) the eccentricity distribution of *Kepler* planets (Xie et al. 2016), discovery of a new population of exoplanets with key properties similar to the hot Jupiters (Dong et al. 2018) and a constraint on the fraction of stars with *Kepler*-like systems (Zhu et al. 2018). With LAMOST-MRS and the new synergy with TESS, we expect that LAMOST data will continue to contribute significantly in the following two

As stars are commonly formed in binary systems, studying planets in binaries is important to understand the general process of planet formation. However, existing observations of planets in binaries are incomplete and biased. Radial velocity (RV) exoplanet surveys usually avoid binaries in the initial target selection. Although at the target selection stage, transit surveys like *Kepler* and TESS are not particularly biased against binaries, transit observations alone typically only yield limited constraints on binaries from detecting eclipses for binary companions at relatively close separations with orbital planes well aligned with the line of sight. High-resolution direct-imaging follows up of transit targets with adaptive optics have revealed that a significant portion exoplanets hosts are wide binaries (e.g., Law et al. 2014). LAMOST-MRS can achieve a radial velocity precision of  $\sim 1$  km/s, and in complementary with high-resolution imaging observations, LAMOST-MRS RV follow-up data can reveal binary companions at close and intermediate separations at nearly all orbital orientations.

TESS is an all-sky survey, which can potentially find exoplanets across various stellar types and populations. With the large samples accessible to LAMOST-MRS and additional astrometric information from *Gaia*, it is also possible to probe the Galactic distribution of planets (thin disk vs. thick disk) using metallicity and kinematics information. In particular, LAMOST-MRS could measure the abundances of more element than LAMOST low-resolution data, e.g.,  $\alpha$  elements [ $\alpha/\text{Fe}$ ], which can aid the stellar population diagnostic (Zhang et al. 2019). Based on our current knowledge of the structure of thin and thick disks (e.g., Bland-Hawthorn & Gerhard, 2016), we expect that  $\sim 10\%$  of our targets are thick-disk stars, and the LAMOST-MRS TESS synergy may find  $\sim 100$  or more planet systems around thick-disk stars. Statistical studies by comparing the exoplanet systems of different star populations will provide new insight into planet formation during the history of the Galaxy evolution.

## 2.7 Open clusters

Open clusters (OCs) have long been used to trace the structure and evolution of the Galactic disk. Open clusters have large age and distance spans and can be relatively accurately dated; the spatial distribution and kinematical properties of OCs provide critical constraints on the overall structure and dynamical evolution of the Galactic disk. Meanwhile, their [M/H] values serve as excellent tracers of the abundance gradient along the Galactic disk, as well as many other important disk properties, such as the age-metallicity relation (AMR), abundance gradient evolution, etc.

With the great ability of LAMOST-MRS, we expect to survey dozens of open clusters to obtain stellar radial velocities as well as abundance information of around  $3 \times 10^5$  stars complete to  $G \sim 15$  mag to cover the cluster central areas as well as their surrounding fields. This will give the largest magnitude-complete spectroscopic dataset for studying the Milky Way open clusters. Meanwhile, the observations for total of  $3 \times 10^5$  stars nearly uniformly distributed around the open clusters will provide most extending and well-representative cluster-halo sample with spectroscopic data, which would be of great importance for probing the overall spatial structure and dynamical evolution of open clusters (e.g., Zhong et al. 2019).

The large amount of up-to-date homogeneous open cluster data from LAMOST-MRS will lead to the most reliable membership determination for sample clusters using accurate radial velocity, combining with

diagrams of sample open clusters, obtaining the essential parameters of clusters, such as distances and ages, and also provide the best basis for investigating internal kinematic properties of open clusters.

Our target samples contain a large portion of young ( $\log t \leq 7.5$ ) clusters. Young open clusters, which retain a representative mass spectrum, are favorable targets to determine the IMF. However, in the absence of spectroscopic data IMF determinations are subject to uncertainties in the slope measurements and contamination. Meanwhile, only limited spectroscopic surveys to young clusters have been conducted to date.

From LAMOST-MRS survey, based on most reliably kinematic-based membership estimation and together with precise Gaia DR2 photometric data, comprehensive photometry and spectroscopy of hundreds of members in each of young clusters will be obtained. This will result in unprecedented improvements in the study of IMF as well as the formation and early evolution of star clusters.

### 3 THE SURVEY STRATEGY AND PLAN

In this section, we present the expected survey performance, survey strategy and plan.

#### 3.1 Expected performance

We have been conducting a commissioning survey between October 2017 and June 2018 and obtained about 5 million single exposure medium-resolution stellar spectra. We tested different exposure time from 600 to 1800 s and finally decide to take 1200 s as the default exposure time, which can provide a balance between the signal-to-noise ratio (S/N) of single exposure and limiting magnitude. Figure 1 shows how S/N of the medium-resolution spectra changes with *Gaia* *G*-band magnitude for around 5 million 1200 s exposure spectra observed during the commissioning survey. The left panel shows that, in the blue band, the S/N is larger than 5 when  $G < 14.5$  mag. In the right panel, the limiting magnitude can go down to 15 mag when  $S/N = 5$ . When we co-add three single 1200 s-exposure-spectra for common stars and re-calculate the S/N of the co-added spectra, we find the S/N of blue band of these co-added spectra is around 10 at  $G = 14.5$  mag. At  $G \sim 13.5$ , the blue band S/N is around 20, at which we can obtain chemical elemental abundance statistically. At  $G \sim 12$  mag, the blue band S/N reaches 50, which is enable to provide reliable elemental abundances for individual stars. Table 1 lists the S/Ns for blue and red bands for single 1200 s exposure and co-added  $3 \times 1200$  s exposure time as functions of *G* magnitude.

It is noted that a few spectra with smaller magnitudes have lower S/N than the majorities. This is caused that they were observed by about 20% low-efficiency fibers.

Liu, N. et al. (2019) and Wang et al. (2019) have investigated the performance of the radial velocity derived from cross-identification for LAMOST-MRS spectra. They illustrated that the uncertainty of the radial velocity is around  $1 \text{ km s}^{-1}$ . For the binaries in time-domain spectroscopic data, in principle, we do not need the absolutely calibrated radial velocities. The relatively calibrated radial velocities should be sufficient for many of the time-domain sciences. Therefore, we are developing an independent pipeline to derive the differential radial velocity with correction of the systematic deviation occurred in each exposure. With the relatively calibrated differential radial velocities, the uncertainty of the late-type stars can reach  $\sim 0.2 \text{ km s}^{-1}$  (Xiong et al. in prep), a factor of 5 better than regular radial velocity estimates. Moreover,

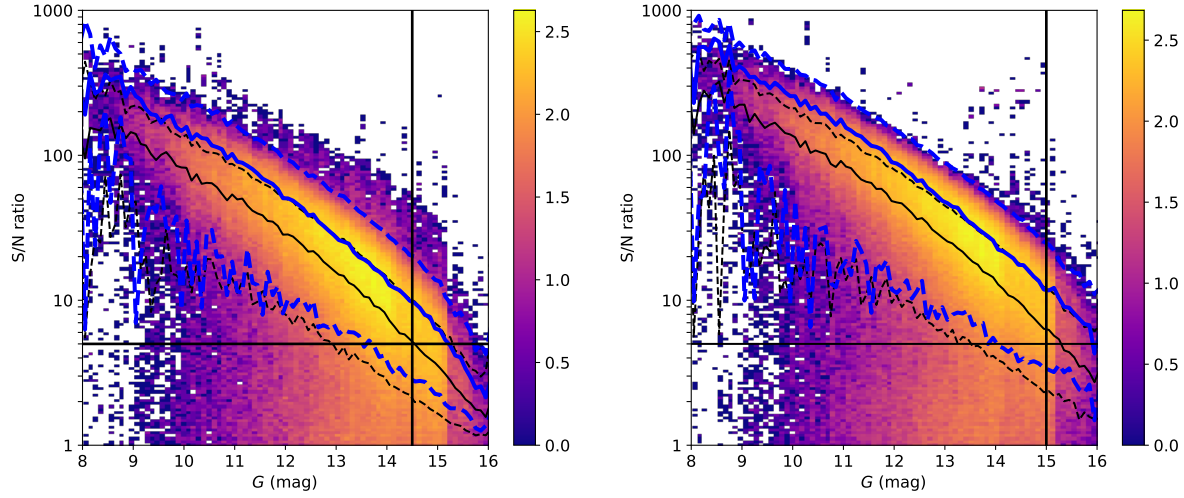


**Fig. 1** The left panel shows the distribution of around 5 million blue-band spectra with single 1200 s exposure in S/N (blue) vs.  $G$  magnitude plane. The colors indicate the logarithmic number of stars in each bin. The black solid and dashed lines show the median S/N and 15% (85%) percentiles along  $G$  magnitude. The thick blue solid and dashed lines show the median S/N and its 15% (85%) percentiles for the co-added spectra with  $3 \times 1200$  s exposure time. The vertical line indicates  $G = 14.5$  mag, at which the single 1200 s exposure reaches median S/N of 5. The horizontal line indicate S/N= 5. The right panel shows the distribution of around 5 million red-band spectra with single 1200 s exposure in S/N (red) vs.  $G$  magnitude plane. The symbols are similar to the left panel. The black vertical line indicates  $G = 15$  mag, which is the limiting magnitude at S/N= 5 at red band.

**Table 1** The signal-to-noise ratio vs.  $G$  magnitude.

$G$ mag	S/N at blue band 1200 s exposure	S/N at red band 1200 s exposure	S/N at blue band $3 \times 1200$ s exposure	S/N at red band $3 \times 1200$ s exposure
11.0	51.60	87.47	96.09	165.53
11.5	39.12	65.10	71.92	120.45
12.0	28.40	47.83	50.50	88.69
12.5	21.73	36.54	38.72	66.86
13.0	15.56	26.25	27.15	47.64
13.5	11.13	19.11	19.48	34.36
14.0	7.74	13.61	13.64	24.05
14.5	5.18	9.46	9.75	17.51
15.0	3.55	6.30	6.30	11.78

measurable change during the observations. These constant stars are widely distributed in all time-domain fields and will be used for absolute calibration of the radial velocities used in the time-domain spectroscopic

### 3.2 Survey strategy

According to the scientific goals, we separate the LAMOST-MRS survey into two parts—the non time-domain and the time-domain survey. The non time-domain (hereafter NT) survey will obtain a few millions of stars widely and roughly continuously distributed in the sky to incorporate with the Galactic archaeology, star forming region, nebulae area etc. Because NT survey does not use the single exposure information, we are able to co-add the single-exposure spectra for a same star to achieve higher S/N. Typically, a NT plate will continuously take 3 single 1200 s exposure and obtain the co-added spectra with total exposure time of  $3 \times 1200$  s. Based on the commissioning survey, this can obtain limiting magnitude of  $G = 14.5$  mag for blue band and 15 mag for red band with  $S/N \sim 10$ .

In the mean time, the time-domain (hereafter TD) survey focuses on some specific pencil beams and repeatedly observe the same groups of stars located in these fields over years. For TD survey, the spectra will be observed with 3–8 single 1200 s exposures in one observation night and will be repeatedly observed many nights during the 5-year survey. For the variation of radial velocities, as we mentioned in section 3.1, the single-exposure spectra will be used. Therefore, the limiting magnitude of the TD survey will reach  $G \sim 14$  mag and 14.5 mag for blue and red bands, respectively, so that the S/N can be higher than  $\sim 10$ . It is noted that the TD single-exposure spectra can also be co-added finally and obtained fairly high S/N for elemental abundance estimation.

Therefore, we plan to set the limiting magnitude of  $G = 15$  mag for both NT and TD surveys.

As seen in section 2, the LAMOST-MRS survey has to combine quite versatile scientific topics within one survey. We hence break down the survey into a few different sub-projects, the *Kepler* region survey (MRS-K), the TESS follow-up survey (MRS-T), the star forming region survey (MRS-S), the binary survey (MRS-B), the Galactic nebulae survey (MRS-N), the Galactic archaeology survey (MRS-G), and open cluster survey (MRS-O). Among them, MRS-K, MRS-T, MRS-B, and part fields of MRS-S are assigned as the TD survey, while the MRS-G, MRS-N, MRS-O, and the rest part of the MRS-S are operated as NT survey.

To determine the best ratio of TD to NT surveys, we run lots of 5-year-survey simulations with different ratios of TD to NT. In the simulations, we assume that if the field to be observed is a NT field, LAMOST will take three continuous 1200 s exposures; if it is a TD field, LAMOST will flexibly take a few 1200 s exposures (at least 3 times, sometimes more, depending on the specific requests of the fields) within the 4-hour observation window around meridian, which is the only sky area that LAMOST is able to observe. While the NT field is continuously distributed in the northern sky, the TD field must be pre-selected as a series of pencil beam sky area. Therefore, we randomly select 100, 200, 300, 400, and 500 TD fields, respectively, in the simulations. The simulations only assign half of a month to LAMOST-MRS survey and leave the other half for the low-resolution survey. The results of the simulations are summarized in Table 2.

Within 5 years, the simulations show that LAMOST-MRS can observe around 2220 NT and TD *visits* together. The term *visit* is defined as following: a) if a TD field is observed in one night, no matter how many exposures it is taken, we count it as 1 visit; b) if a TD field is observed in two nights, we count it as 2

**Table 2** Results of the survey simulations to determine the ratio of TD to NT observations.

Visits of TD		TD/(TD+NT) in visits			
		20%	40%	60%	80%
100	No. of observed fields	99	100	100	100
	Observation visits	701	1184	1609	1939
200	No. of observed fields	192	195	200	199
	Observation visits	707	1202	1601	1936
300	No. of observed fields	264	291	295	298
	Observation visits	707	1199	1617	1954
400	No. of observed fields	316	368	388	389
	Observation visits	707	1199	1615	1943
500	No. of observed fields	373	440	466	477
	Observation visits	710	1196	1609	1951

It is seen from Table 2 that the larger fraction of the TD fields, the more observation visits for each TD field. For instance, when  $TD/(TD + NT) = 20\%$  and we set 100 TD fields in the simulations, we obtain that the observation visits per TD field is  $701/99 \approx 7.1$ . However, when  $TD/(TD + NT) = 80\%$ , the number of visits per TD field increases to  $1939/100 \approx 19.39$ . On the other hand, the more pre-selected TD fields, the less the number of the observed field. In other word, the more TD fields is selected, the less the completeness for each field can reach.

Considering the performance of the orbital resolution of spectroscopic binary stars, we need to at least observe  $\sim 10$  visits per star. We finally adopt that the total number of TD fields is around 100 and the fraction of TD fields is 60% among the all MRS fields by taking into account the least numbers of objects. According to the simulations, in this case, each TD field can be visited 16 times. The  $\sim 100$  TD fields are assigned to MRS-B, MRS-K, MRS-T, and MRS-S. Table 3 lists all pre-selecting TD fields with a flag of which sub-project they belong to.

Note that the survey plan may slightly change during the 5-year survey so that the visits of observations for TD fields can be balanced to each sub-project. It is expected that, through such moderate adjustment, each sub-project can obtain sufficient epochs with proper observation intervals to satisfy its scientific goals.

## 4 DETAILED SURVEY PLAN

### 4.1 Input catalogs

In order to provide a homogeneous input catalog, the LAMOST-MRS survey uses *Gaia* DR2 (Gaia Collaboration et al. 2018) as the basic input catalog. Most of these targets are found in *Gaia*. For some special targets which may not be provided based on *Gaia* data, we cross-identify their *Gaia* counterpart. An exception is the targeting for MRS-N, which plans to observe non-stellar objects. The sub-project sets up its own method for targeting (see Wu et al. in prep.).

### 4.2 Targeting strategies

Figure 2 displays the footprints for the LAMOST-MRS survey. Detailed discussions about the targeting

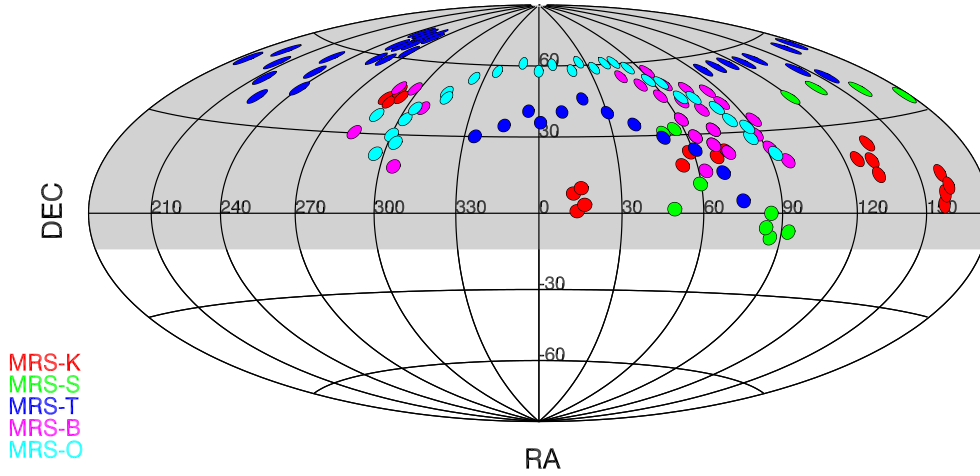


**Fig. 2** The airtoff map shows the footprints of the LAMOST-MRS survey. The gray area indicates the NT footprint.

#### 4.2.1 MRS-B fields

In order to evaluate binary fraction and binary parameters (e.g. orbital period, eccentric, and mass function and so on) accurately, we hope to observe each fields with 16 visits. In the MRS-B sub project, the binaries with periods from a few ten days to several hundred days are paid more attentions, so we try to make sure the observe cadence would larger than a few days and only exposure 3 times, which likes the NT observation projects, within a visit. A fixed cadence could lead to a selection effect in periods. So we do not fix the observation cadence. In addition, we randomly select two fields (TD060648N233818B and TD203106N405128B) that will observe at least one visit in each available month of the future five years observation. In this way, we can obtain more than 16 radial velocities for each source. It would help us to get hundreds of binary parameters with periods around a year.

#### 4.2.2 MRS-K fields

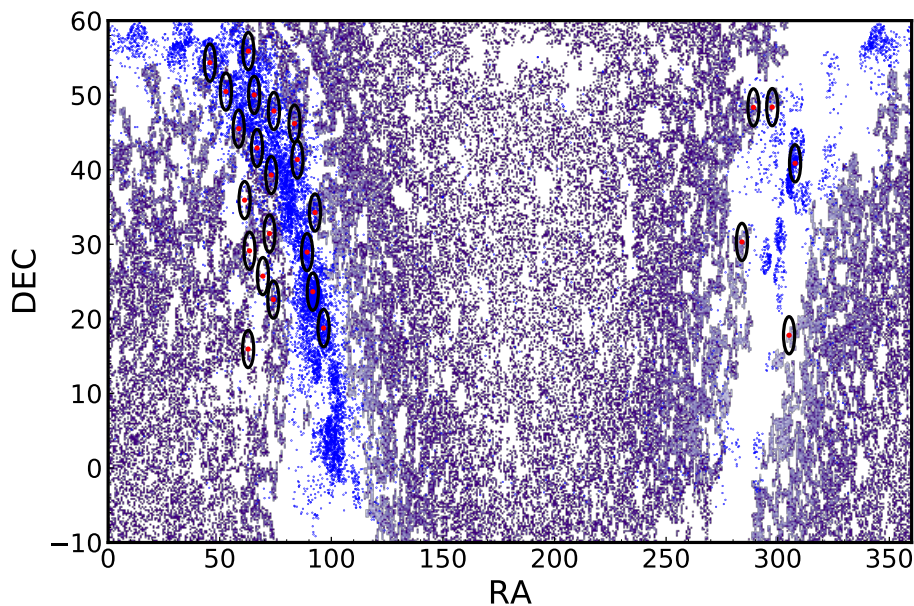
As can be seen from Figure 4, we plan to have LAMOST to make time-domain spectroscopic observations for 20 plates distributed in the *K1* field and four fields of the *K2* mission, i.e. the C08, C04/C13, C05/C16, and C14, with four plates in each field, respectively. On average, each plate will get around 60 exposures during the second five years of LAMOST surveys.

With the observation strategy of the MRS-K sub-project, LAMOST is expected to observe two plates in two neighboring fields in right ascension sequentially with one plate observed continuously for four hours when the plate is passing around the meridian during each night. Typically, two successful visits of LAMOST to each of the two plates in each month are needed while each plate is on the target list for 3 months with around 6 visits for one survey year. In the following survey year, the same plates are re-visited one more time and then move to the next plates in the same *Kepler* fields and so on. In this way, each plate is observed for around eight times, each of which can continuously monitor the field for maximally 4 hours.

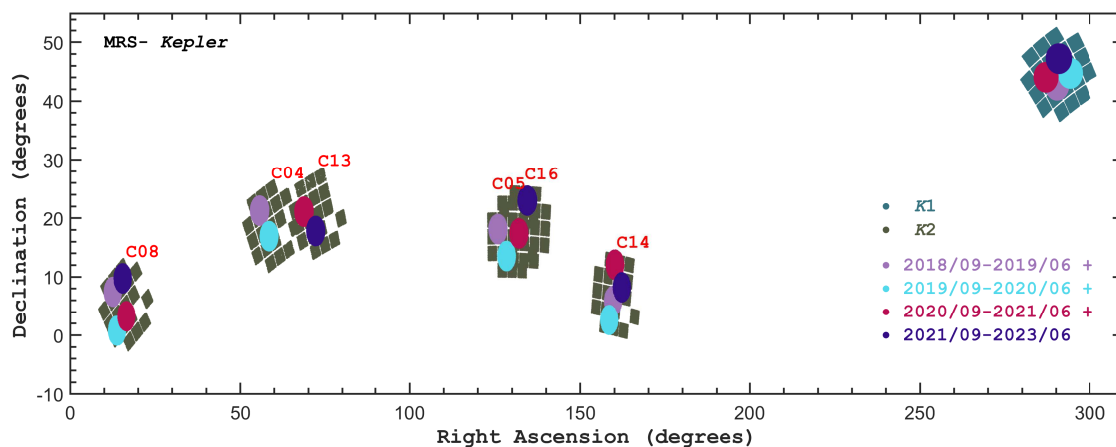
**Table 3** MRS TD fields

Plate Name	RA	dec	Type	Plate Name	RA	dec	Type
TD005004N074006K	12.5179	7.6685	K	TD005501N004722K	13.7558	0.7896	K
TD010142N094445K	15.4287	9.7460	K	TD010605N031628K	16.5241	3.2747	K
TD033722N181216K	54.3451	18.2047	K	TD035321N230725K	58.3382	23.1236	K
TD043446N210613K	68.6954	21.1037	K	TD045334N231856K	73.3921	23.3157	K
TD082325N180811K	125.8576	18.1364	K	TD084806N172341K	132.0265	17.3948	K
TD084844N123545K	132.1871	12.5960	K	TD085754N225914K	134.4779	22.9875	K
TD103356N023723K	158.4834	2.6231	K	TD103827N055449K	159.6151	5.9136	K
TD104037N120443K	160.1555	12.0787	K	TD104844N081314K	162.1836	8.2207	K
TD190808N440210K	287.0347	44.0364	K	TD192102N424113K	290.2617	42.6870	K
TD192314N471144K	290.8118	47.1958	K	TD193637N444141K	294.1582	44.6949	K
TD031711N013329S	49.2994	1.5581	S	TD032323N305902S	50.8497	30.9840	S
TD034419N321717S	56.0797	32.2882	S	TD035837N110139S	59.6556	11.0275	S
TD040433N355514S	61.1407	35.9206	S	TD041324N290722S	63.3519	29.1229	S
TD043724N254338S	69.3525	25.7274	S	TD044912N312614S	72.3035	31.4374	S
TD053531S051602S	83.8807	-5.2674	S	TD054232S000057S	85.6372	-0.0161	S
TD054339S085615S	85.9138	-8.9378	S	TD061101S064515S	92.7551	-6.7542	S
TD080016N404735S	120.0691	40.7931	S	TD091555N422558S	138.9804	42.4328	S
TD103949N392416S	159.9556	39.4047	S	TD114941N345554S	177.4238	34.9318	S
TD000246N354855T	0.6917	35.8154	T	TD004049N401113T	10.2054	40.1870	T
TD012220N453143T	20.5852	45.5288	T	TD020047N393731T	30.1984	39.6254	T
TD024017N343505T	40.0735	34.5849	T	TD032020N290254T	50.0849	29.0485	T
TD040421N240621T	61.0904	24.1059	T	TD043731N150847T	69.3832	15.1465	T
TD050047N043403T	75.1969	4.5676	T	TD062018N541459T	95.0789	54.2498	T
TD070113N545124T	105.3067	54.8567	T	TD073820N551219T	114.5837	55.2055	T
TD081828N543349T	124.6203	54.5638	T	TD085722N545046T	134.3433	54.8462	T
TD094225N484633T	145.6042	48.7761	T	TD101631N450236T	154.1301	45.0435	T
TD110230N550142T	165.6279	55.0286	T	TD114018N551809T	175.0786	55.3027	T
TD121948N485902T	184.9529	48.9841	T	TD125617N540558T	194.0717	54.0997	T
TD134023N503110T	205.0968	50.5194	T	TD141602N453358T	214.0100	45.5663	T
TD145924N393841T	224.8540	39.6449	T	TD151257N560247T	228.2412	56.0465	T
TD153834N502523T	234.6425	50.4233	T	TD160011N441646T	240.0493	44.2796	T
TD161932N702206T	244.8867	70.3685	T	TD164021N701415T	250.0889	70.2376	T
TD164055N643520T	250.2297	64.5890	T	TD165902N691110T	254.7607	69.1863	T
TD165950N582745T	254.9587	58.4626	T	TD170215N643602T	255.5655	64.6007	T
TD171857N704716T	259.7396	70.7878	T	TD172042N653823T	260.1753	65.6400	T
TD172604N583906T	261.5202	58.6519	T	TD174016N690900T	265.0704	69.1503	T
TD174903N624755T	267.2661	62.7988	T	TD221648N300528T	334.2007	30.0913	T
TD230151N343645T	345.4644	34.6125	T	TD234129N403316T	355.3734	40.5545	T
TD030224N542147B	45.6017	54.3633	B	TD033106N502853B	52.7775	50.4816	B
TD035400N453042B	58.5035	45.5118	B	TD040433N355514B	61.1407	35.9206	B
TD041055N155648B	62.7299	15.9467	B	TD041114N555437B	62.8103	55.9105	B
TD041324N290722B	63.3518	29.1229	B	TD042145N500206B	65.4395	50.0352	B
TD042649N425435B	66.7056	42.9099	B	TD043724N254338B	69.3524	25.7274	B
TD044912N312615B	72.3035	31.4376	B	TD045227N391703B	73.1158	39.2842	B
TD045606N223436B	74.0275	22.5767	B	TD045704N475243B	74.2692	47.8788	B
TD053403N461112B	83.5141	46.1869	B	TD053908N412131B	84.7863	41.3589	B
TD055633N285632B	89.1407	28.9423	B	TD060648N233818B	91.7027	23.6386	B
TD061044N341537B	92.6860	34.2604	B	TD062610N184526B	96.5430	18.7573	B
TD185549N301843B	283.9552	30.3121	B	TD191631N482124B	289.1298	48.3568	B
TD195013N482329B	297.5549	48.3916	B	TD202021N174734B	305.0892	17.7930	B
TD203106N405128B	307.7787	40.8579	B				

observed. Each star is expected to have around 60 measurements with two visits per month during the 3 months observations within a year with additional one more visit in the following year. This enables one to search for both the short- and long-term radial velocity variations of stars. Once the plate had been visited at about 60 epochs, that plate will be removed from the entire observational plan. During the practice of observation, this rigorous observational plan might not be followed exactly due to some competition with other parallel programs. We refer one to see the details of the observational results from the first year in



**Fig. 3** 25 plates (black oval circles) with center stars (red solid dots) and four specific plates (red circles) for MRS-B sub-project. The blue dots represent the early stars with O or B spectral types and the purple dots denote the stars with GALEX observations.



**Fig. 4** The spatial distribution of the 20 plates selected for MRS-K sub-project in the *Kepler* fields. They are divided into 4 groups, with each contains 5 plates, each of which will be observed in different years (marked in different colors).

As far as the priorities of the targets, the known pulsating stars, binary stars, stars with stellar activities and exoplanet-host stars will be on the list of top priorities. The fibers will be assigned to stars with available *Kepler* light curves in highest priority. The rest fibers are assigned to stars according to their brightness,

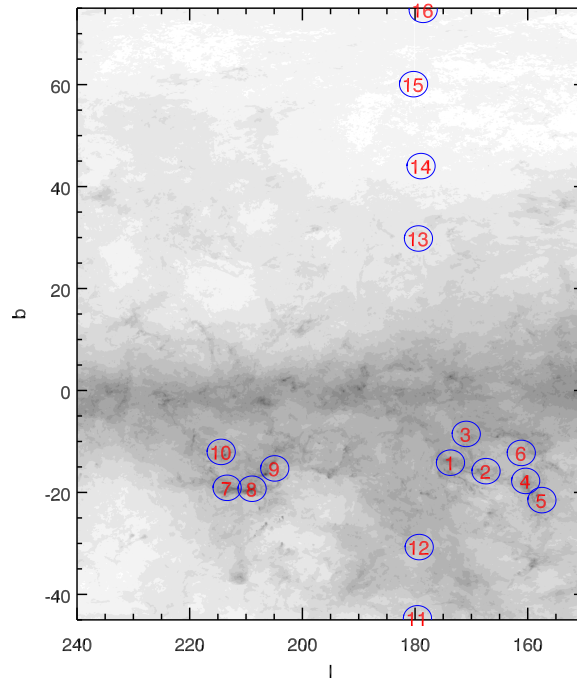


**Fig. 5** The circles indicate the planning fields for the MRS-S TD survey. The gray background displays the dust map of the region. The figure is drawn in Galactic coordinates.

#### 4.2.3 MRS-T fields

We plan to monitor  $\sim 10^5$  TESS stars over the course of  $\sim 5$  years with LAMOST-MRS to constrain the presence of binary companions. Furthermore, for a significant fraction of our sample, we will also benefit from existing *Gaia* RV measurements to extend the accessible binary period range. LAMOST-MRS and TESS synergy will potentially reveal many planet-bearing binary stars and yield the frequency of exoplanets with binary companions, shedding new light into planet formation and evolution in binaries.

#### 4.2.4 MRS-S TD fields

To identify binary stars in very young stellar populations, we plan to operate time-domain spectroscopic survey in the nearby star forming regions. However, because the large area of these regions, we can only select a few fields so that we can achieve the survey within 5 years. Figure 5 shows the location of the selected fields with the interstellar dust map as background. The field numbers from 1 to 6 covers the Taurus and Perseus star forming regions. The numbers from 7 to 10 covers part of the Orion region. And the field from 11 to 16 are located at different Galactic latitudes so that they can provide control samples with different stellar populations. Identified young pre-main sequence stars located within these fields are marked as highest priority so that MRS-S survey can have more targets for the young stars.

The strategy of the time-domain observations for the MRS-S TD fields is the same as that of the MRS-B

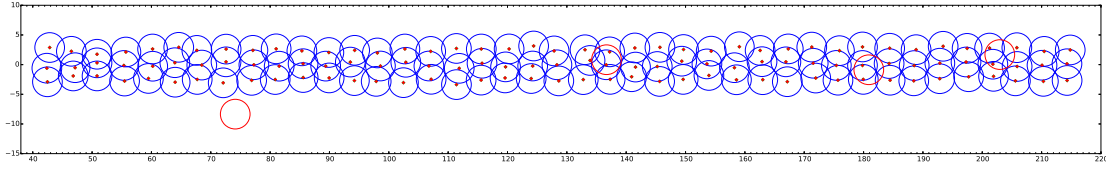


**Fig. 6** 123 GP plates (blue circles) with center stars (red plus) and four specific plates (red circles) for MRS-N sub-project. The  $x$ -axis is Galactic longitude and  $y$ -axis is Galactic latitude.

#### 4.2.5 MRS-N fields

From commissioning observations, we have concluded that MRS-N is seriously affected by the moonlight. So all the observation time of MRS-N should be assigned into a time range when the altitude of moon is lower than  $-1^\circ$ .

The survey areas of MRS-N include two parts, the Galactic plane (GP) areas and four specific areas (see Fig. 6). The GP areas cover the northern plane within the Galactic longitude range  $40^\circ < l < 215^\circ$  and the latitude range  $-5^\circ < b < 5^\circ$ , about 1700 square degrees. Four specific areas are Westerhout 5 (HII region), Rosette Nebula+NGC2264 (HII region), Cygnus Loop (SNRs) and Simeis 147 (SNRs), respectively.

We plan to use 123 plates to cover the GP areas. The exposure time of each plate is  $3 \times 900$  seconds. For each specific area, the exposure time is designed as  $16 \times 900$  seconds. So it will take about 130 hours to finish the whole MRS-N survey. MRS-N will be assigned 30 hours per year. So we can finish the MRS-N survey within 5 years without considering other objective factor such as weather.

Because MRS-N mainly focus on the spectra of non-point source (such as the structure of nebulae), the input catalogs should be made independently unlike other LAMOST-MRS sub-projects. The input catalogs of four specific areas are man-made by comparing with optical images. From optical images, some bright stars, some sky areas and the positions of interesting structure of nebulae are selected to compose input catalogs. While the input catalog of GP area is very complex. Here we divide GP area into about 1.5 million  $2 \times 2$  arcmin grids. Each grid can be considered as the moving area of each fiber. Then we cross-match the 1.5 million grids with Hipparcos main catalog and Pan-STARRS1 (PS1). If a star within a grid is brighter than 13 magnitude, then the star is selected as location of fiber with objtype STAR. If a star within a grid is brighter than 18 and fainter than 13, then the location of fiber within the same grid should avoid the star. Else if there is not a star in a grid or the star is too faint to observe, then the location of fiber should be pointed to the brightest position within the grid.

#### 4.2.6 MRS-O fields

In order to obtain a large number of spectra of cluster members in the LAMOST-MRS, we selected 18 open cluster related fields (hereafter OCs fields, as seen in Fig. 7 which contain several tens of OCs with as many members as possible to perform the MRS-O spectroscopic observation. For each OCs field, we arranged 8 plates for observation with same center star but different fiber positions to increase the completeness of

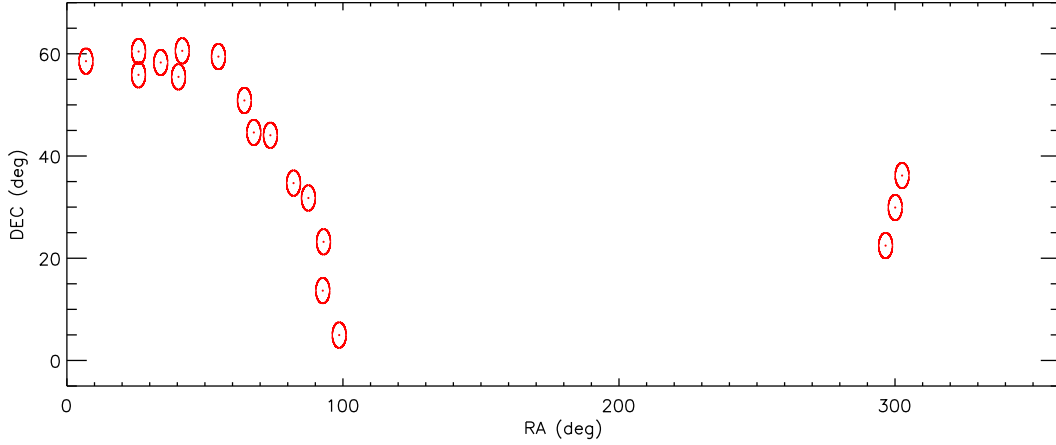


**Fig. 7** 18 MRS-O fields with center stars (red dots) in celestial coordinates (Right Ascension and Declination). Fields are designed to cover OCs and members as many as possible.

time of each MRS-O plate is  $3 \times 1200$  s. It is noted that the completeness of obtained cluster members will increase to 80% through 8 plates of spectroscopic observations, down to  $G=15$ mag.

Since most of OCs are located on the Galactic plane, our 18 OCs fields are mainly arranged on the low Galactic latitude and along the Galactic longitude as evenly as possible. Figure 7 shows the spatial distribution of the selected OCs fields. Considering the observation mode of LAMOST, most of MRS-O plates will be observed during the period from September to February.

#### 4.2.7 MRS-G fields

In general, MRS-G sub-project does not have special sky area as high priority, but continuously cover the all available sky as LAMOST low-resolution survey has been doing. The limiting magnitude of the targets for MRS-G is  $G = 15$  mag. The selection function of the targets is in principle the same as the previous low-resolution survey (Carlin et al. 2012, Liu et al. 2017a).

Same as other input catalog of the other LAMOST MRS fields, most of the targets in MRS-G filed are selected from the *Gaia* DR2 catalog. We use the ‘square degree’ as the basic block for evaluating the upper-limit of the source density in the sky. Considering a total of 4,000 fibers and a field-of-view (FOV) of 20 square degrees for LAMOST, we set an upper-limit source density of 500 stars per square degree for MRS-G field. This means for each sky area of 20 square degrees, there will be approximately 10,000 targets of maximum to be observed, which can be arranged within three plates.

In Figure 8, we show the number density of the stars with  $G$  magnitude between 9.0 and 15.0 mag in the *Gaia* catalog. It is clear that the density of stars varies with the Galactic latitude. For a large fraction area of the sky, the density is below 500 stars per square degree, in such sky areas, all the targets were selected into our input catalog. While for the higher density regions, a series criterions were applied to generate 500 stars as the sources for the input catalog. In general, we use the color of  $bp-rp$  as the filter. We first generate a grid in the dimensions of  $G$  magnitude v.s.  $bp-rp$ . The step in  $G$  magnitude dimension is always 0.5 mag,

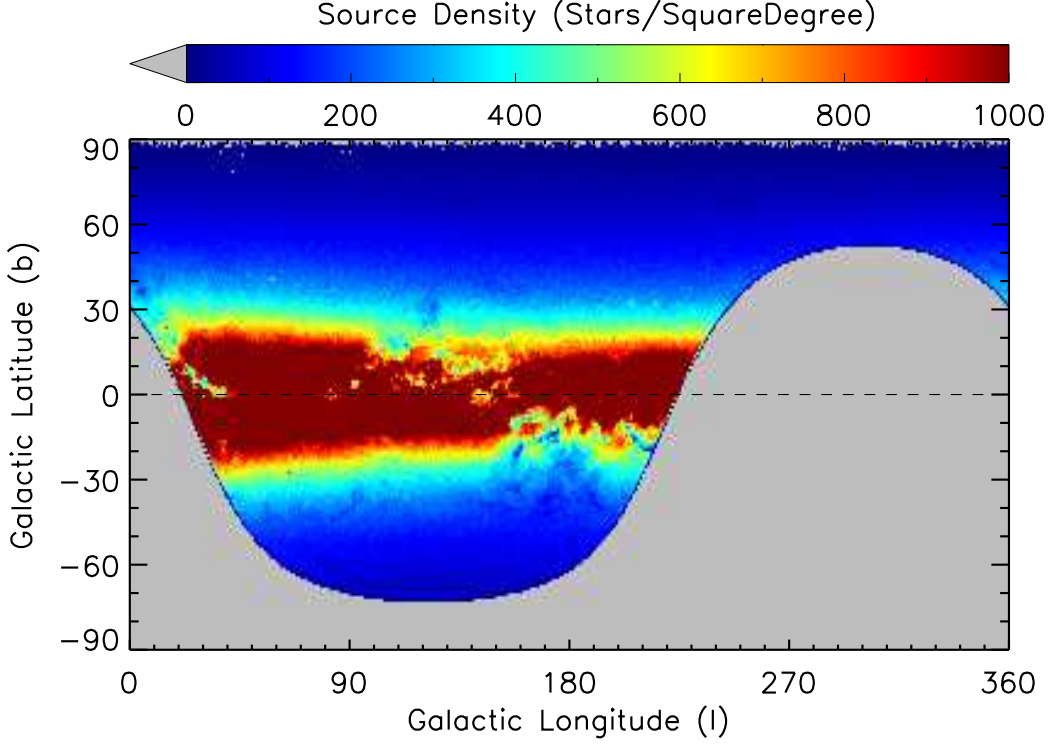


**Fig. 8** The number density of stars with  $G$  magnitude between 9.0 to 15.0 mag in a Galactic coordinates map. Colors indicate different density, as illustrated on top of the figure. Although the Galactic plane is much more dense with stars, we set the upper-boundary of the density as 1,000 for a better visual effects.

- 1)  $bp - rp < 0.0$  mag: treated as a single step
- 2)  $0.0 \leq bp - rp < 6.0$  mag: 0.5 mag for each step
- 3)  $bp - rp \geq 6.0$  mag: treated as a single step

Thus, we got a grid with  $12 \times 14 = 168$  bins in the  $G$  v.s.  $bp-rp$  space. For the stars in the bins of  $bp-rp < 0.0$  and  $bp-rp \geq 6.0$ , we consider them as stars of ‘color peculiarity’, and they were always selected into our ‘pool’ of 500 stars. While for the other bins, one target is randomly selected from each bin for each time to be filled into the ‘pool’, and this procedure continually repeats until there is not enough space for filling with one star from each bin. Then we fill the ‘pool’ to 500 stars with the targets selected from random, non-repeating bins throughout the grid. The selection function thus can be corrected given the known number of stars for each color bin. Figure 9 shows an example of target selecting for an over-dense area of one square degree sky. The number density of our final input catalog of MRS-G is shown in Figure 10.

## 5 SUMMARY

As one of the largest spectroscopic survey over the world, LAMOST started to conduct medium-resolution spectroscopic survey and will significantly increase the number of stellar spectra with medium-resolution. In general, medium-resolution stellar spectra can provide more precise radial velocity as well as more information in the spectra, such as rotational velocity, elemental abundance, emission line profile etc. These

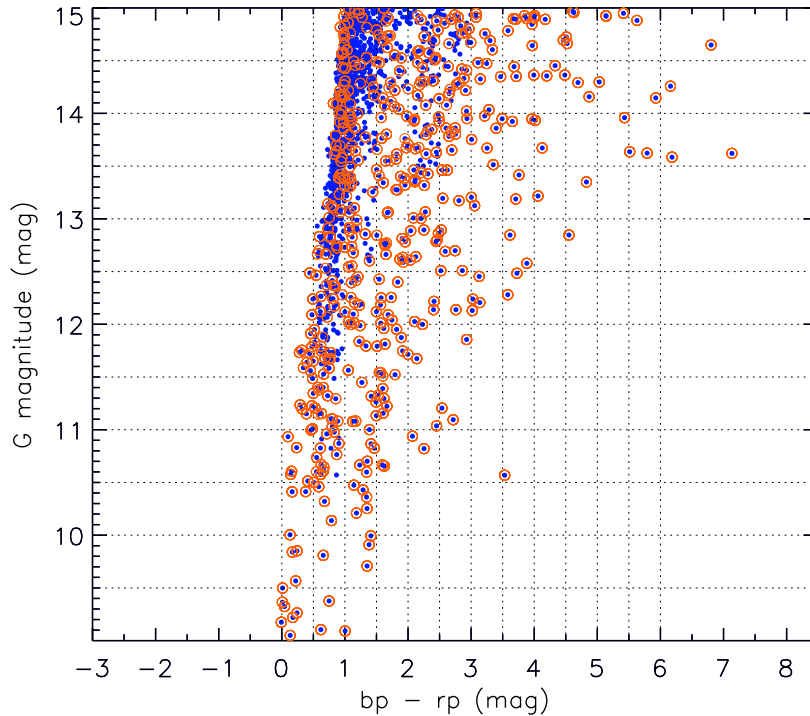


**Fig. 9** An example of target selecting for an over-dense area of one square degree sky. This is an area near the Galactic plane with a total of  $\sim 1,500$  stars. The blue dots indicate all the stars in this area, and the red circle indicate which stars are selected. The grid is shown with dotted lines. The criterion of selection ensures that the stars that are bluer or redder than the majority will be always selected into our catalog.

Galactic archaeology, emission nebula etc. Thus, LAMOST-MRS is able to expand the sciences from the Milky Way to more about the stellar physics and nebulae physics. Moreover, LAMOST-MRS will conduct time-domain spectroscopic survey in its 5-year survey plan. This will provide around 200 thousand stars with averagely 60 exposures. Such a large time-domain dataset will leverage the science about binary stars and variable stars in the next five years and may get some breakthrough in these topics.

**Acknowledgements** This work is supported by National Key R&D Program of China No. 2019YFA0405500. CL thanks the National Natural Science Foundation of China (NSFC) with grant No. 11835057. JRS and HLY acknowledge the supports from the Astronomical Big Data Joint Research Center, co-founded by the National Astronomical Observatories, Chinese Academy of Sciences and the Alibaba Cloud. CHH acknowledges the supports from The Science and Technology Development Fund, Macau SAR (file no. 0007/2019/A) and Faculty Research Grants of the Macau University of Science and Technology (program no. FRG-19-004-SSI). HNL acknowledges NSFC grant No. 11973049 and the Strategic Priority Research Program of Chinese Academy of Sciences, Grant No. XDB34020205. This work is also partly funded by NSFC grant No. 11833002, 11733006, 11903048, U1631131, 11973060, 11973001, 11773009,

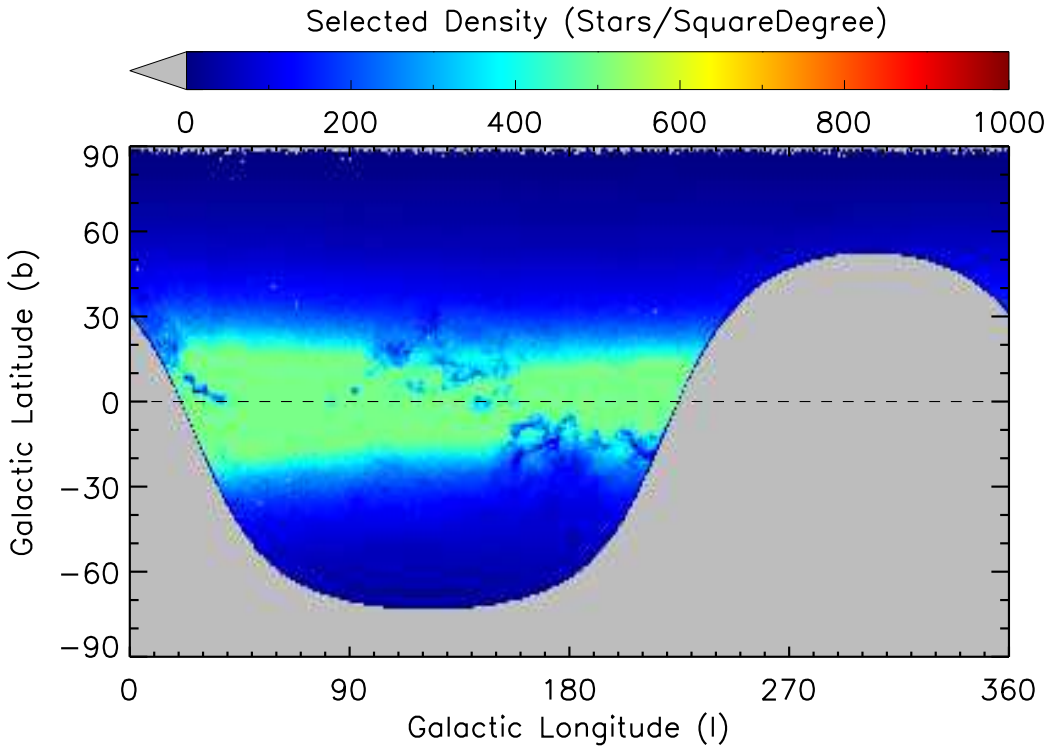


**Fig. 10** The number density of targets in MRS-G input catalog in a Galactic coordinates map. Colors are same as Figure 8.

Guoshoujing Telescope (the Large Sky Area Multi-Object Fiber Spectroscopic Telescope LAMOST) is a National Major Scientific Project built by the Chinese Academy of Sciences. Funding for the project has been provided by the National Development and Reform Commission. LAMOST is operated and managed by the National Astronomical Observatories, Chinese Academy of Sciences.

## References

- Abbott, B.P., et al. 2016, *PhRvL*, 116, 061102
- Aerts, C., Christensen-Dalsgaard, J., & Kurtz, D. W. 2010, *Asteroseismology*, Astronomy and Astrophysics Library. ISBN 978-1-4020-5178-4. Springer
- Afflerbach, A., Churchwell, E., & Werner, M. W. 1997, *ApJ*, 478, 190
- Allen, G. E., Houck, J. C., & Sturmer, S. J. 2008, *ApJ*, 683, 773
- Ambartsumian, V. A. 1954, in *Liege International Astrophysical Colloquia*, Vol. 5, Liege International Astrophysical Colloquia, 293
- Arbutina, B. 2017, *Publications de l'Observatoire Astronomique de Beograd*, 97, 1
- Bally, J. 2016, *ARA&A*, 54, 491
- Balsler, D. S., Rood, R. T., Bania, T. M., & Anderson, L. D. 2011, *ApJ*, 738, 27
- Barentsen, G., Farnhill, H. J., Drew, J. E., et al. 2014, *MNRAS*, 444, 3230
- Blair, W. P., & Long, K. S. 2004, *ApJS*, 155, 101
- Bland-Hawthorn, J., & Gerhard, O. 2016, *ARA&A*, 54, 529
- Borucki, W. J., Koch, D., Basri, G., et al. 2010, *Science*, 327, 977
- Breger M., 1990, *Comm. in Asteroseismology*, 20, 1 (Univ. of Vienna)
- Carlin, J. L., Lépine, S., Newberg, H. J., et al. 2012, *Research in Astronomy and Astrophysics*, 12, 755
- Chen X., Han Z., 2009, *MNRAS*, 395, 1822
- Chen, X., Han, Z., Deca, J., et al. 2013, *MNRAS*, 434, 186

- Chiappini, C., Matteucci, F., & Gratton, R. 1997, *ApJ*, 477, 765
- Chiappini, C., Matteucci, F., & Romano, D. 2001, *ApJ*, 554, 1044
- Cudworth, K. M., & Herbig, G. 1979, *AJ*, 84, 548
- Cui, X.-Q., Zhao, Y.-H., Chu, Y.-Q., et al. 2012, *Research in Astronomy and Astrophysics*, 12, 1197
- De Cat, P., Fu, J. N., Ren, A. B., et al. 2015, *ApJS*, 220, 19
- Deharveng, L., Peña, M., Caplan, J., & Costero, R. 2000, *MNRAS*, 311, 329
- De Marco, O., Izzard, R.G., 2017, *PASA*, 34, 1
- Deng, L.-C., Newberg, H. J., Liu, C., et al. 2012, *Research in Astronomy and Astrophysics*, 12, 735
- Dong, S., Zheng, Z., Zhu, Z., et al. 2014, *ApJ*, 789, L3
- Dong, S., Xie, J.-W., Zhou, J.-L., Zheng, Z., & Luo, A. 2018, *PNAS*, 115, 266
- Drew, J. E., Greimel, R., & Irwin, M. J., et al. 2005, *MNRAS*, 362, 753
- Duchêne, G., & Kraus, A. 2013, *ARA&A*, 51, 269
- Duquennoy, A., & Mayor, M. 1991, *A&A*, 500, 337
- Dyson, J. E. 1979, *A&A*, 73, 132
- El-Badry, K., & Rix, H.-W. 2019, *MNRAS*, 482, L139
- El-Badry, K., Rix, H.-W., Tian, H., et al. 2019, *MNRAS*, 489, 5822
- Esteban, C., García-Rojas, J., Peimbert, M., et al. 2005, *ApJ*, 618, L95
- Esteban, C., Carigi, L., Copetti, M. V. F., et al. 2013, *MNRAS*, 433, 382
- Esteban, C., Fang, X., García-Rojas, J., & Toribio San Cipriano, L. 2017, *MNRAS*, 471, 987
- Fesen, R. A., Blair, W. P., & Kirshner, R. P. 1985, *ApJ*, 292, 29
- Fernández-Martín, A., Pérez-Montero, E., Vílchez, J. M., & Mampaso, A. 2017, *A&A*, 597, A84
- Fich, M., & Silkey, M. 1991, *ApJ*, 366, 107
- Fuentes-Masip, O., Muñoz-Tuñón, C., Castañeda, H. O., & Tenorio-Tagle, G. 2000, *AJ*, 120, 752
- Gaia Collaboration, Prusti, T., de Bruijne, J. H. J., et al. 2016, *A&A*, 595, A1
- Gaia Collaboration, Brown, A. G. A., Vallenari, A., et al. 2018, *A&A*, 616, A1
- Gao, S., Liu, C., Zhang, X., et al. 2014, *ApJ*, 788, L37
- Giammichele, N., Charpinet, S., Fontaine, G., et al. 2018, *Nature*, 554, 73
- Green, D. A. 2014, in *IAU Symposium*, Vol. 296, *Supernova Environmental Impacts*, ed. A. Ray & R. A. McCray, 188
- Green, D. A. 2015, in *Astrophysics and Space Science Proceedings*, Vol. 43, *New Insights From Recent Studies in Historical Astronomy: Following in the Footsteps of F. Richard Stephenson*, ed. W. Orchiston, D. A. Green, & R. Strom, 91
- Gu, W.-M., Mu, H.-J., Fu, J.-B., et al. 2019, *ApJ*, 872, L20
- Han, Z., Podsiadlowski, P., & Eggleton, P. P. 1995, *MNRAS*, 272, 800
- Han, Z., Eggleton, P. P., Podsiadlowski, P., et al. 1995, *MNRAS*, 277, 1443
- Han, Z. 1998, *MNRAS*, 296, 1019
- Han, Z., Podsiadlowski, P., Maxted, P. F. L., et al. 2002, *MNRAS*, 336, 449
- Han, Z., & Podsiadlowski, P. 2004, *MNRAS*, 350, 1301
- Hillwig, T.C., Bond, H.E., De Marco, O. 2010, *AJ*, 140, 319
- Hsia, C.-H., & Zhang, Y. 2014, *A&A*, 563, A63
- Huang, Y., Liu, X.-W., Yuan, H.-B., et al. 2016, *MNRAS*, 463, 2623
- Huang, Y., Zhang, H.W., Wang, C., et al. 2019, *ApJ*, 884, L7
- Iben I.Jr., Tutukova A.V. 1984, *ApJS*, 54, 335
- Jones, D., Boffin, H.M.J. 2017, *Nature Astronomy*, 1, 0117
- Karoff, C., Knudsen, M. F., De Cat, P., et al. 2016, *Nature Communications*, 7, 11058
- Kennicutt, R. C., Jr., & Chu, Y.-H. 1988, *AJ*, 95, 720
- Korotin, S. A., Andrievsky, S. M., Luck, R. E., et al. 2014, *MNRAS*, 444, 3301
- Kohoutek, L. 2001, *A&A*, 378, 843
- Kratter, K. M., Matzner, C. D., & Krumholz, M. R. 2008, *ApJ*, 681, 375
- Kratter, K. M., Matzner, C. D., Krumholz, M. R., et al. 2010, *ApJ*, 708, 1585
- Lada, C. J., & Lada, E. A. 2003, *ARA&A*, 41, 57
- Law, N. M., Morton, T., Baranec, C., et al. 2014, *ApJ*, 791, 35
- Li, J., FELLOW, . (LAMOST ., Liu, C., et al. 2019, *ApJ*, 874, 138
- Li, H., Tan, K., & Zhao, G. 2018, *ApJS*, 238, 16

- Liang, X.-long., Zhao, J.-kun., Chen, Y.-qin., et al. 2018, *Chinese Astronomy and Astrophysics*, 42, 1
- Lissauer, J. J., Dawson, R. I., & Tremaine, S. 2014, *Nature*, 513, 336
- Liu, C., Fang, M., Wu, Y., et al. 2015, *ApJ*, 807, 4
- Liu, C., Xu, Y., Wan, J.-C., et al. 2017a, *Research in Astronomy and Astrophysics*, 17, 096
- Liu, C., Wang, Y.-G., Shen, J., et al. 2017b, *ApJ*, 835, L18
- Liu, C. 2019, *MNRAS*, 490, 550
- Liu, J., Zhang, H., Howard, A. W., et al. 2019, *Nature*, 575, 618
- Liu, N., Fu, J.-N., Zong, W., et al. 2019, *Research in Astronomy and Astrophysics*, 19, 075
- Livio, M. 2000, in *Type Ia Supernovae: Theory and Cosmology*, ed. J.C. Niemeyer & J.W. Truran (Cambridge Univ. press) P.33
- Long, K. 2016, *What Makes Radio-detected and Optically-detected Supernova Remnants in NGC6946 Different?*, HST Proposal
- Luo, A.-L., Zhao, Y.-H., Zhao, G., et al. 2015, *Research in Astronomy and Astrophysics*, 15, 1095
- Luo, Y.-P., Németh, P., Liu, C., et al. 2016, *ApJ*, 818, 202
- Machida, M. N., Omukai, K., Matsumoto, T., et al. 2009, *MNRAS*, 399, 1255
- Maoz, D., Mannucci, F., Nelemans, G. 2014, *ARA&A*, 52, 107
- Mao, Y.-W., Lin, L., & Kong, X. 2018, *ApJ*, 853, 151
- Marks, M., & Kroupa, P. 2011, *MNRAS*, 417, 1702
- Masci, F. J., Laher, R. R., Rusholme, B., et al. 2019, *PASP*, 131, 018003
- Miszalski, B., Parker, Q. A., Acker, A., et al. 2008, *MNRAS*, 384, 525
- Moe, M., & Kratter, K. M. 2018, *ApJ*, 854, 44
- Moe, M., Kratter, K. M., & Badenes, C. 2019, *ApJ*, 875, 61
- Monreal-Ibero, A., Relaño, M., Kehrig, C., et al. 2011, *MNRAS*, 413, 2242
- Morgan, D. P., West, A. A., Garcés, A., et al. 2012, *AJ*, 144, 93
- Murphy, S. J., Moe, M., Kurtz, D. W., et al. 2018, *MNRAS*, 474, 4322
- Mundt, R. 1985, *The Observatory*, 105, 224
- Mundt, R. 1987, *Mitteilungen der Astronomischen Gesellschaft Hamburg*, 70, 100
- Napiwotzki, R., Edelmann, H., Heber U. et al. 2001, *A&A*, 378, 17
- Paczynski, B. 1976, *IAUS*, 73, 75
- Parker, Q. A., Acker, A., Frew, D. J., et al. 2006, *MNRAS*, 373, 79
- Pérez-Montero, E. 2017, *PASP*, 129, 043001
- Raghavan, D., McAlister, H. A., Henry, T. J., et al. 2010, *ApJS*, 190, 1
- Ren, A., Fu, J., De Cat, P., et al. 2016, *ApJS*, 225, 28
- Ren, J.-J., Liu, X.-W., Chen, B.-Q., et al. 2018, *arXiv:1804.10989*
- Ricker, G. R., Winn, J. N., Vanderspek, R., et al. 2014, *Proc. SPIE*, 9143, 914320
- Rudolph, A. L., Fich, M., Bell, G. R., et al. 2006, *ApJS*, 162, 346
- Sana, H. et al. 2012, *Sci.*, 337, 444
- Schwartz, R. D. 1975, *ApJ*, 195, 631
- Schwartz, R. D. 1983, *rmxaa*, 7, 27
- Searle, L. 1971, *ApJ*, 168, 327
- Shaver, P. A., McGee, R. X., Newton, L. M., Danks, A. C., & Pottasch, S. R. 1983, *MNRAS*, 204, 53
- Shen, S.-Y., Argudo-Fernández, M., Chen, L., et al. 2016, *Research in Astronomy and Astrophysics*, 16, 43
- Simpson, J. P., Colgan, S. W. J., Rubin, R. H., Erickson, E. F., & Haas, M. R. 1995, *ApJ*, 444, 721
- Smith, M. G., & Weedman, D. W. 1970, *ApJ*, 161, 33
- Stutz, A. M., & Gould, A. 2016, *A&A*, 590, A2
- Tanaka, K. E. I., & Omukai, K. 2014, *MNRAS*, 439, 1884
- Tenorio-Tagle, G., Munoz-Tunon, C., & Cid-Fernandes, R. 1996, *ApJ*, 456, 264
- Terlevich, R., & Melnick, J. 1981, *MNRAS*, 195, 839
- Tian, H.-J., Liu, C., Carlin, J. L., et al. 2015, *ApJ*, 809, 145
- Tian, H.-J., Liu, C., Wan, J.-C., et al. 2017, *Research in Astronomy and Astrophysics*, 17, 114
- Tian, H.-J., Liu, C., Wu, Y., et al. 2018, *ApJ*, 865, L19
- Tian, H.-J., El-Badry, K., Rix, H.-W., et al. 2019, *arXiv e-prints*, *arXiv:1909.04765*
- Tian, H., Liu, C., Xu, Y., et al. 2019, *ApJ*, 871, 184

- Vucetic, M. M., Arbutina, B., & Urosevic, D. 2015, *VizieR Online Data Catalog*, 744
- Wang, L., Wang, W., Wu, Y., et al. 2016, *AJ*, 152, 6
- Wang, S., Bai, Y., Zhang, C.-P., et al. 2017, *Research in Astronomy and Astrophysics*, 17, 10
- Wang, Q., Wang, Y., Liu, C., et al. 2017, *MNRAS*, 470, 2949
- Wang, H.-F., Liu, C., Xu, Y., et al. 2018, *MNRAS*, 478, 3367
- Wang, L.-L., Luo, A.-L., Hou, W., Wang, M.-X., Du, B., Qin, L., Han, J.-S. 2018, submitted to *ApJ*
- Wang, C., Huang, Y., Yuan, H.-B., et al. 2019, *ApJ*, 877, L7
- Wang, C., Liu, X.-W., Xiang, M.-S., et al. 2019, *MNRAS*, 482, 2189
- Wang, R., Luo, A.-L., Chen, J.-J., et al. 2019, *ApJS*, 244, 27
- Webbink, R.F. 1984, *ApJ*, 277, 355
- Whelan, J., Iben, I.Jr. 1973, *ApJ*, 186, 1007
- Woltjer, L. 1972, *ARA&A*, 10, 129
- Wu, X.-B., Chen, Z.-Y., Jia, Z.-D., et al. 2010, *Research in Astronomy and Astrophysics*, 10, 737
- Wu, X.-B., Jia, Z.-D., Chen, Z.-Y., et al. 2010, *Research in Astronomy and Astrophysics*, 10, 745
- Wu, C.-J., Wu, H., Hsia, C.-H., et al. 2020, *Research in Astronomy and Astrophysics*, 20, 033
- Xiang, M.-S., Liu, X.-W., Yuan, H.-B., et al. 2015, *Research in Astronomy and Astrophysics*, 15, 1209
- Xie, J.-W., Dong, S., Zhu, Z., et al. 2016, *PNAS*, 113, 11431
- Xu, Y., Liu, C., Xue, X.-X., et al. 2018, *MNRAS*, 473, 1244
- Yu, J., & Liu, C. 2018, *MNRAS*, 475, 1093
- Zhang, B., Liu, C., Li, C.-Q., et al. 2019, arXiv e-prints, arXiv:1910.13154
- Zhang, B., Liu, C., & Deng, L.-C. 2020, *ApJS*, 246, 9
- Zhang, L.-Y., Long L., Shi J.-R., et al., 2020, *MNRAS*, in press
- Zhao, G., Zhao, Y.-H., Chu, Y.-Q., et al. 2012, *Research in Astronomy and Astrophysics*, 12, 723
- Zhao, J. K., Zhao, G., Aoki, W., et al. 2018, *ApJ*, 868, 105
- Zhu, W., Petrovich, C., Wu, Y., Dong, S., & Xie, J. 2018, *ApJ*, 860, 101
- Zhong, J., Chen, L., Kouwenhoven, M. B. N., et al. 2019, *A&A*, 624, A34
- Zong, W., Fu, J.-N., De Cat, P., et al. 2018, *ApJS*, 238, 30
- Zong, W., Fu, J.-N., De Cat, P., et al. 2020, *ApJS*, Submitted